International Journal of Applied Earth Observation and Geoinformation 32 (2014) 67–78

Contents lists available at ScienceDirect

International Journal of Applied Earth Observation and Geoinformation

journal homepage: www.elsevier.com/locate/jag

Assessing the effects of land use spatial structure on urban heat islands using HJ-1B remote sensing imagery in Wuhan, China

Hao Wu[a,b], Lu-Ping Ye[a], Wen-Zhong Shi[b,*], Keith C. Clarke[c]

[a] School of Resources and Environmental Engineering, Wuhan University of Technology, Wuhan 430070, PR China
[b] Department of Land Surveying and Geo-Informatics, The Hong Kong Polytechnic University, Hunghom, Kowloon, Hong Kong
[c] Department of Geography, University of California, Santa Barbara, Santa Barbara 93106, USA

ARTICLE INFO

Article history:
Received 6 November 2013
Accepted 26 March 2014
Available online 21 April 2014

Keywords:
Urban heat island
Land use spatial structure
Vegetation indexes
Landscape metrics
Fractal analysis
HJ-1B

ABSTRACT

Urban heat islands (UHIs) have attracted attention around the world because they profoundly affect biological diversity and human life. Assessing the effects of the spatial structure of land use on UHIs is essential to better understanding and improving the ecological consequences of urbanization. This paper presents the radius fractal dimension to quantify the spatial variation of different land use types around the hot centers. By integrating remote sensing images from the newly launched HJ-1B satellite system, vegetation indexes, landscape metrics and fractal dimension, the effects of land use patterns on the urban thermal environment in Wuhan were comprehensively explored. The vegetation indexes and landscape metrics of the HJ-1B and other remote sensing satellites were compared and analyzed to validate the performance of the HJ-1B. The results have showed that land surface temperature (LST) is negatively related to only positive normalized difference vegetation index (NDVI) but to Fv across the entire range of values, which indicates that fractional vegetation (Fv) is an appropriate predictor of LST more than NDVI in forest areas. Furthermore, the mean LST is highly correlated with four class-based metrics and three landscape-based metrics, which suggests that the landscape composition and the spatial configuration both influence UHIs. All of them demonstrate that the HJ-1B satellite has a comparable capacity for UHI studies as other commonly used remote sensing satellites. The results of the fractal analysis show that the density of built-up areas sharply decreases from the hot centers to the edges of these areas, while the densities of water, forest and cropland increase. These relationships reveal that water, like forest and cropland, has a significant effect in mitigating UHIs in Wuhan due to its large spatial extent and homogeneous spatial distribution. These findings not only confirm the applicability and effectiveness of the HJ-1B satellite system for studying UHIs but also reveal the impacts of the spatial structure of land use on UHIs, which is helpful for improving the planning and management of the urban environment.

Introduction

Many developing countries around the world are experiencing rapid urbanization. Continued urbanization has caused fundamental changes in land use and the landscape pattern over the past two decades (Turkoglu, 2010; Weng, 2007). These changes have led to a series of ecological and environmental issues and seriously threaten the sustainable development of urban areas. Among these problems, the urban heat island (UHI) is a major issue (Hage, 2003; Streutker, 2003; Weng, 2001, 2003; Xian and Crane, 2006). The UHI is the phenomenon where land surface temperatures are higher in urban areas than in the rural surroundings (Arnfield, 2003; Voogt and Oke, 2003). It has caused significant impacts on the daily life of city dwellers, including extreme heat, sandstorms and seasonal epidemics. Several studies have focused on identifying the factors that contribute to UHIs (Chen et al., 2006; House-Peters and Chang, 2011; Kardinal Jusuf et al., 2007; Li et al., 2012b; Lo and Quattrochi, 2003; Oke, 1973; Saaroni et al., 2000; Streutker, 2002; Taha, 1997; Weng et al., 2004; Zhou et al., 2011a).

The land surface temperature is a universal and important parameter for analyzing UHIs (Aguiar et al., 2002; Ma et al., 2010; Mallick et al., 2012; Sobrino et al., 2012). The UHI is generally evaluated in two ways. Traditionally, UHIs have been measured by ground-based observations taken from automobile transects and weather station networks (Voogt and Oke, 2003). With the development of thermal remote sensors, satellite-based imaging technology is now widely applied to detect UHIs both remotely and regionally because it can offer a straightforward and consistent

* Corresponding author. Tel.: +852 2766 5975; fax: +852 2330 2994.
E-mail address: lswzshi@polyu.edu.hk (W.-Z. Shi).

http://dx.doi.org/10.1016/j.jag.2014.03.019
0303-2434/

approach to determining the spatial–temporal distribution of LST (Streutker, 2003). In the early stage, NOAA AVHRR and EOS MODIS were used to derive land surface temperature to study urban heat islands (Cui and De Foy, 2012; Friedl et al., 2002; Gallo and Owen, 1998; Streutker, 2003), but their spatial resolutions are too coarse to analyze variations in UHIs with precision. Numerous studies based on Landsat TM/ETM+ data have recently been conducted (Gao et al., 2011; Li et al., 2012a; Tan et al., 2012; Xu et al., 2009; Zhang et al., 2009; Zhao et al., 2012). Due to its low revisiting frequency (16 days), however, it is difficult to characterize and examine UHIs consistently or to monitor UHIs in real time. In this context, the satellite revisit time has been regarded as a bottleneck problem for UHI studies because remote sensing imagery has a high spatial resolution but a relatively low temporal resolution (Streutker, 2003; Wu et al., 2014). The time interval and gap of at-satellite thermal sensors make the dynamics and patterns of UHIs appear more complex than other factors (Li et al., 2009). Fortunately, the availability of HJ-1B remote sensing satellite imagery, which has a high revisiting frequency of no more than 4 days in China since 2008, has significantly improved the ability to examine the spatial–temporal features of UHIs and the understanding of the correlations associated with the spatial structure of land use. One important advantage of using HJ-1B TIR data is that its spatial resolution (300 m) is higher than that of MODIS TIR data (1000 m), although it only provides an image every four days, while MODIS obtains data twice daily over the same locations via the Terra and Aqua satellites. In contrast, the HJ-1B TIR data have coarser resolution but a higher frequency than that of Landsat TM/ETM+. Furthermore, the HJ-1B TIR sensors can capture more subtle changes in land surface temperatures than Landsat TM/ETM+ because of its higher pixel quantization (Yang et al., 2010). Given its temporal resolution and spatial resolution, the TIR sensor of the HJ-1B satellite has great potential in urban studies.

Previous studies have found that different land use types can produce remarkably heterogeneous effects on UHIs that have been assessed using various methods (Van De Kerchove et al., 2013; Weng et al., 2008; Weng and Lu, 2008). For instance, LST has significant negative correlations with the normalized difference vegetation index (NDVI) (Liang and Weng, 2011; Tran et al., 2006) as well as fractional vegetation cover (Fv) through vegetation indexes, while LST positively correlates to impervious surface area (Dousset and Gourmelon, 2003; Wilson et al., 2003). Nevertheless, few systematic investigations and validations have been performed to verify whether the same tendency and relationships exist for HJ-1B data, although a considerable amount of work has been performed to retrieve LST from the data. Regardless of how sophisticated the satellite instruments are, remote sensors that are well designed and calibrated prior to launch gradually degrade with time because of thermal, mechanical and electrical effects or exposure to UV radiation. Because it is a newly launched remote sensing satellite, evaluating the performance of HJ-1B in characterizing urban thermal environments by comparing it with commonly used remote sensors is critical to our ability to rapidly and accurately monitor the spatial variation of urban heat islands in China (Ye et al., 2013).

The method of performing quantitative analyses is another key factor to determine whether the effect of land use structure on the urban thermal environment can be comprehensively and effectively assessed directly from thematic maps. Actually, the analysis method is more important than the availability of remote sensing imagery with shorter revisit times. Landscape metrics are environmental variables that have commonly been used to describe spatial patterns of the land surface (Herzog and Lausch, 2001; Roy et al., 2005). Because they can reveal spatial features of land use that are not directly observable, landscape metrics can link the spatial variations in land surface temperatures to differences in land use patterns. However, because of the spatial heterogeneity and hierarchical properties of these patterns, it is difficult to assess the effects of different land use structures across a range of scales using a single analysis method. Recently, a series of fractal analysis methods have been increasingly regarded as potential tools for studying urban heat islands (Li et al., 2009; Weng, 2003; Wilson et al., 2003; Chen et al., 2007). Weng (2003) first used fractal analysis to detect temporal changes in UHIs and proved it to be an effective spatial measure by computing the fractal dimensions of three transects with the divider method in Guangzhou, China. Later, Weng et al. (2004) extended the technique with additional transects to investigate the relationship between LST and vegetation abundance. Chen et al. (2006) evaluated three fractal models (the surface, profile and pixel models) to determine their suitability for analyzing the structure and dynamics of urban heat islands. Li et al. (2009) performed a four-direction analysis through the Hausdorff–Besicovitch dimension and indicated that the spatial dependency of the UHIs in Shanghai was mainly related to the structural variance in an E–S profile. Although fractal analysis has had success in examining the spatial variations of urban heat islands, no substantial research has yet studied the spatial patterns of land use around high temperature centers using fractal analysis, particularly to assess the effects of different land use spatial structures around the hot centers of urban heat islands.

Wuhan City is one of the Three Furnaces (Li and Yu, 2008) and is the most rapidly urbanizing metropolis in Central China. This paper uses Wuhan City as a case study to assess the effects of urban heat islands in response to land use patterns from rapid urbanization by integrating remote sensing imagery, vegetation indexes, landscape metrics and the fractal dimension. Considering the potential of monitoring UHIs using the HJ-1B satellite, this study gives an explicit contrast analysis to those results from other remote sensing satellites so as to validate its good performance. Specifically, this study provides a comprehensive examination of the relationship between different land use types and land surface temperature variations and quantitatively assesses the contributions of the spatial structure of land use to the urban heat island effect using fractal analysis. The overall objective of our manuscript is to provide a positively auxiliary function toward the sustainable development of urban area.

Study area and data

Study area

Wuhan, which is the capital of Hubei Province, is the largest city along the middle part of the Yangtze River and lies between 113°41′ and 115°05′ E longitude and between 29°58′ and 31°22′ N latitude (Fig. 1). The administrative area of Wuhan covers almost 8494 km^2 and contains a central district that covers 888 km^2 and rural districts that cover 7606 km^2. Its metropolitan area is divided into three parts by the Yangtze River and Han River, including Hanyang, Wuchang and Hankou. Wuhan, similar to Shanghai, Beijing and Guangzhou, has witnessed rapid urbanization over the last three decades. The urbanization results in not only the rapid expansion of built areas but also large modifications to the landscape structure, which causes many serious impacts to the urban ecological environment. Of these effects, the UHI is the most important and dramatic reflection of rapid urbanization.

Image and image pre-processing

The HJ-1B image used in this study was provided by the China Center for Resources Satellite Data and Application (CRESDA). The HJ-1B satellite, which was launched on September 6, 2008, carries two CCD cameras and one IRS camera (Table 1). The data are characterized by excellent image quality, stable radiation properties and

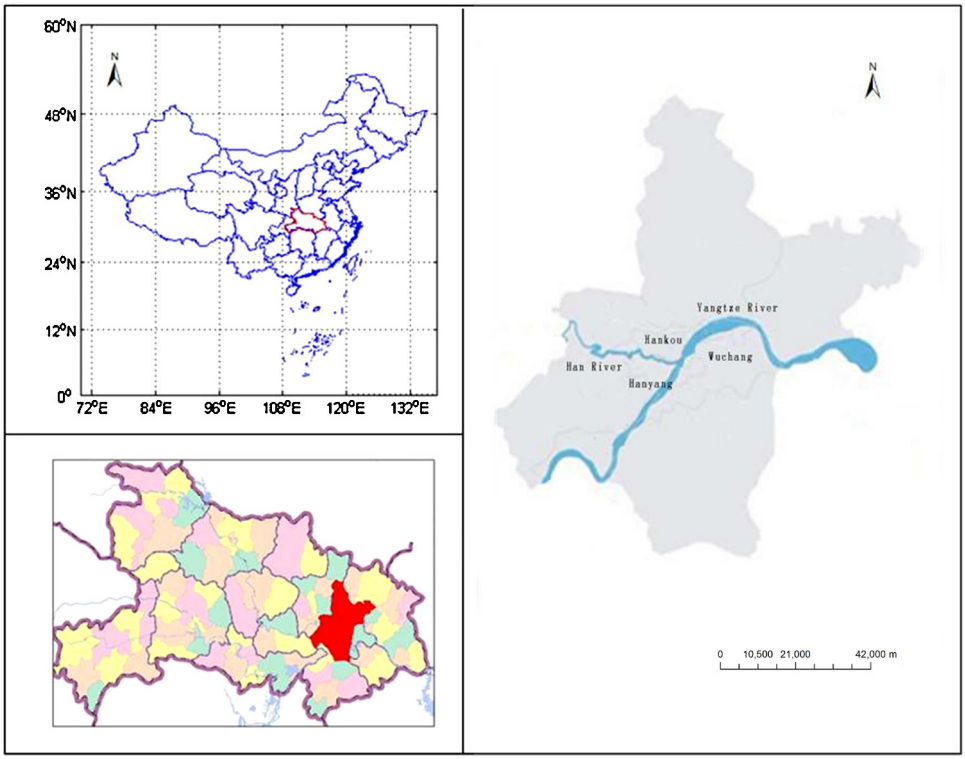

Fig. 1. Location of the study area.

a high revisiting frequency over China (Wang et al., 2010), which make the data suitable for eco-environment monitoring. A scene of HJ-1B data (row/path: 80/454) of Wuhan captured on July 09, 2011 was used to derive the land surface temperature from the IRS imagery and land use classifications from the CCD imagery.

ERDAS Image 9.1 and ENVI 4.5 were used to pre-process the HJ-1B image. The image was rectified to the UTM projection system (ellipsoid WGS84, datum NAD84, zone 49) and was resampled by a third order polynomial with the nearest neighbor method. The digital numbers of the thermal bands were converted to at-sensor radiance using the following equation (Zhao et al., 2011):

$$L_\lambda = \frac{DN_\lambda - offset}{Gain_\lambda} \quad (1)$$

where L_λ is the at-sensor radiance, DN_λ is the digital number of a given pixel, *offset* is the intercept of the *radiance*/*DN* conversion function and $Gain_\lambda$ is the slope of the *radiance*/*DN* conversion function. The values of *offset* and $Gain_\lambda$ are available in the metadata associated with each HJ-1B image. To improve the accuracy of the retrieval temperature, the FLAASH module of ENVI was used for the atmospheric correction of the remote sensing image.

Table 1
Band information of HJ-1B satellite.

Sensor	Band	Spectral range (μm)	Spatial resolution (m)
CCD	1	0.43–0.52	30
	2	0.52–0.60	
	3	0.63–0.69	
	4	0.76–0.90	
IRS	1	0.75–1.10	150
	2	1.55–1.75	
	3	3.50–3.90	
	4	10.5–12.5	300

The HJ-1B CCD image was classified into five land use types, including cropland, water, forest, built-up areas, and bare land. Because each land use type may be composed of various objects with different reflectance characteristics, an ISODATA classifier was used to detect subclasses with the unsupervised clustering method in advance. The maximum likelihood classification was then used to further improve the extraction of the land use (Wu et al., 2012). The result of the land use classification is shown in Fig. 2(a). The kappa coefficient and the overall accuracy of the classification were 0.83 and 86.13%, respectively.

Methods

Computation of NDVI and Fv

As for HJ-1B image, NDVI was expressed as:

$$\mathrm{NDVI} = \frac{\rho_4 - \rho_3}{\rho_4 + \rho_3} \quad (2)$$

where ρ_4 is the reflectance of the near-infrared band and ρ_3 is the reflectance of the red band. The NDVI derived from the HJ-1B image is shown in Fig. 3(a).

The fractional vegetation (Fv) of each pixel was determined from the NDVI using the following equation (Carlson and Ripley, 1997):

$$\mathrm{Fv} = \left(\frac{\mathrm{NDVI} - \mathrm{NDVI_s}}{\mathrm{NDVI_v} - \mathrm{NDVI_s}}\right)^2 \quad (3)$$

where $\mathrm{NDVI_s}$ is the NDVI value of pure soil (0.05) and $\mathrm{NDVI_v}$ is the NDVI value of pure vegetation (0.7). To compute consistent values of Fv, it is necessary to set pixels with $\mathrm{NDVI} > \mathrm{NDVI_v}$ to 1 and pixels with $\mathrm{NDVI} < \mathrm{NDVI_s}$ to zero (Sobrino et al., 2004). The fractional vegetation cover map is shown in Fig. 3(b).

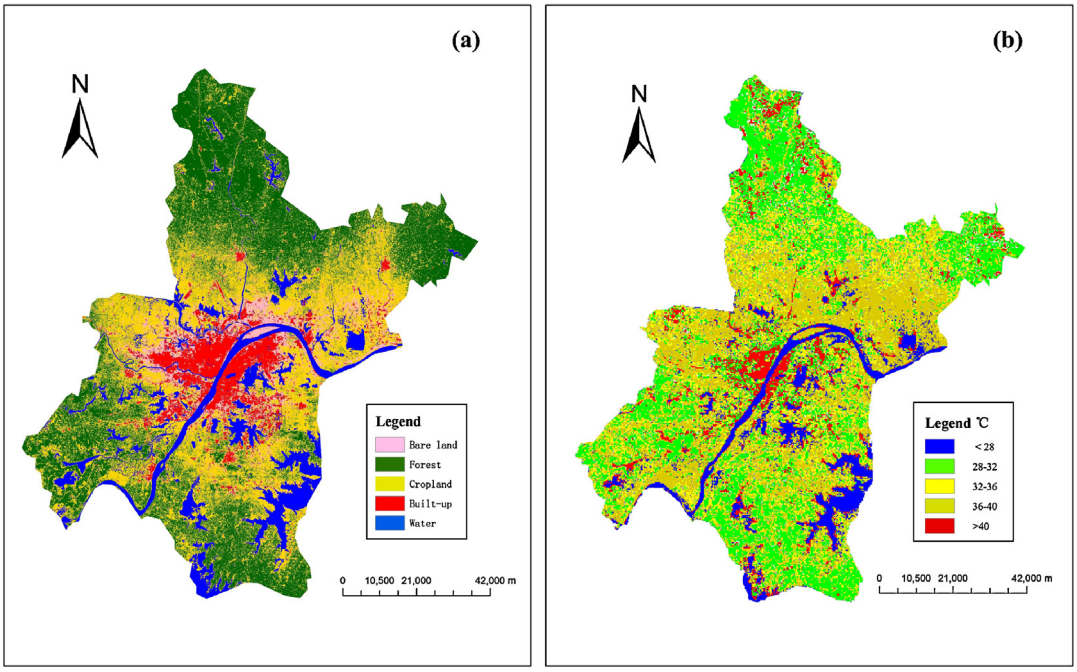

Fig. 2. Land use and Land surface temperature (LST) derived form HJ-1B image for the study area: (a) land use map and (b) LST map.

Land surface temperature retrieval

The HJ-1B thermal infrared band (10.5–12.5 μm) data were radiometrically and geometrically corrected and were then used to derive the land surface temperature of Wuhan. The steps of the land surface temperature retrieval process are as follows.

The digital numbers of the thermal band were first converted to the at-sensor radiance using Eq. (1) and then to the at-sensor brightness temperature. The conversion formula is expressed in Eq. (4):

$$T_b = \frac{K_2}{ln(K_1/L_\lambda)} + 1 \tag{4}$$

where T_b is the at-sensor brightness temperature in Kelvin. For the HJ-1B remote sensor, K_1 is 579.20 W m^{-2} ster^{-1} μm^{-1} and K_2 is 1245.58 K, which are the calibration constants. In addition, L_λ is defined in Eq. (1). The next step is to convert the brightness temperature to land surface temperature. The derivation of the temperature image is described in detail by (Weng et al., 2004) and uses the following equation:

$$T_s = \frac{T_b}{(1 + (\lambda_{eff} \times T_b/C) \ln \varepsilon)} \tag{5}$$

where T_s is the land surface temperature, T_b is the at-sensor brightness temperature from Eq. (4) and the wavelength of the emitted

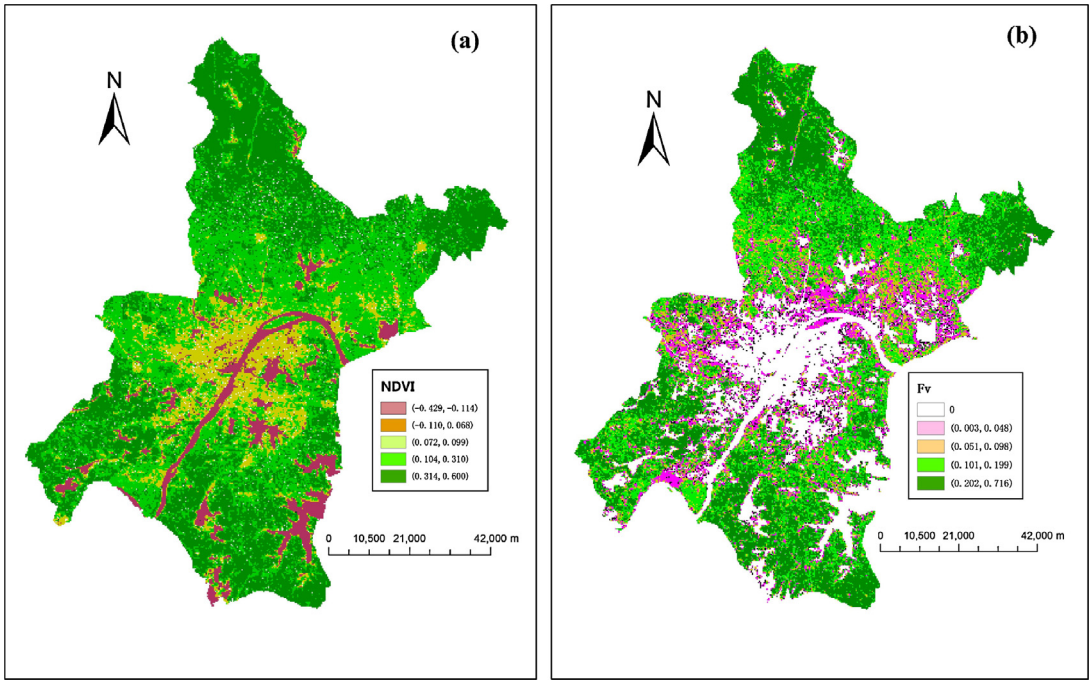

Fig. 3. Normalized difference vegetation index (NDVI) and fractional vegetation cover (Fv) derived form HJ-1B image for the study area: (a) NDVI and (b) Fv.

Table 2
List of landscape metrics used in the study (McGarigal et al., 2002).

Metrics (abbreviation)	Definition	Computing equation
Percentage of landscape (PLAND)	The proportion of total area occupied by a particular land use type	$\mathrm{PLAND} = P_i = \frac{\sum_{j=1}^{n} a_{ij}}{A} \times 100$
Patch density (PD)	The number of patches per 100 ha of the corresponding patch type divided by total landscape area	$\mathrm{PD} = \frac{n_i \times 10000}{A} \times 100$
Edge density (ED)	The sum of the lengths of all edge segments per ha involving the corresponding patch type, divided by the total landscape area	$\mathrm{ED} = \frac{\sum_{k=1}^{m} e_{ik}}{A} \times 10,000$
Landscape shape index (LSI)	The total length of edge in the landscape divided by the minimum total length of edge possible	$\mathrm{LSI} = \frac{0.25 \sum_{k=1}^{m} e'_{ik}}{\sqrt{A}}$
Contagion index (CONTAG)	Aggregation of all patch types	$\mathrm{CONTAG} = \left\{ 1 + \frac{\sum_{i=1}^{m} \sum_{k=1}^{m} \left[P_i \times \left(g_{ik} / \sum_{k=1}^{m} g_{ik} \right) \right] \times \left[\ln \left(P_i \times \left(g_{ik} / \sum_{k=1}^{m} g_{ik} \right) \right) \right]}{2 \ln(m)} \right\} \times 100$
Shannon's diversity index (SHDI)	Diversity in the whole community ecology	$\mathrm{SHDI} = -\sum_{i=1}^{m} (P_i \times \ln P_i)$
Shannon's evenness index (SHEI)	A measurement of patch diversity, which is determined by the distribution of the proportion of different land use types in a landscape.	$\mathrm{SHEI} = -\sum_{i=1}^{m} (P_i \times \ln P_i) / \ln(m)$

radiance λ_{eff} is defined as $\int \lambda f(\lambda) d\lambda / \int f(\lambda) d\lambda$ (Yu et al., 2012). Due to the frequent unavailability of the filter response $f(\lambda)$, the central wavelength is substituted for λ_{eff} despite some errors (Jimenez-Munoz and Sobrino, 2003). The constant C was calculated with the expression $h \times c/\sigma$, where h is Planck's constant (6.626×10^{-34} J s), c is the velocity of light (2.998×10^{8} m/s) and σ is Boltzmann's constant (1.380×10^{-23} J/K). The surface emissivity ε, which is more complicated than the variables described above, was determined for three cases using the NDVI Thresholds Method (Sobrino et al., 2001, 2004; Wang et al., 2011).

(a) $\mathrm{NDVI} < \mathrm{NDVI}_{\min}$

where $\mathrm{NDVI}_{\min}$ is the minimum of NDVI and its value is 0.2. In this case, the pixel was regarded as bare soil and ε was determined by the reflectivity values in the red region:

$$\varepsilon = a\rho + d \tag{6}$$

where ρ is the surface emissivity of the CCD's red region and a and d are the regression coefficients. By combining the reflectance values for different earth surface materials with the related region's spectrum-response function of the HJ-1B CCD cameras, we computed the emissivity of bare soil and the red region. For CCD1, $a = -0.0274$ and $d = 0.9779$, while for CCD2, $a = -0.0273$ and $d = 0.9779$ (Salisbury and D'Aria, 1992; Zhou et al., 2011b).

(b) $\mathrm{NDVI} > \mathrm{NDVI}_{\max}$

where $\mathrm{NDVI}_{\max}$ is the maximum of NDVI and its value is 0.5. In this case, the pixels were considered to be heavily vegetated and ε was derived from the emissivity of vegetation.

(c) $\mathrm{NDVI}_{\min} \le \mathrm{NDVI} \le \mathrm{NDVI}_{\max}$

$$\varepsilon = \varepsilon_v \mathrm{Fv} + \varepsilon_s(1 - \mathrm{Fv}) + d\varepsilon \tag{7}$$

where ε_v is the emissivity of vegetation, ε_s is the emissivity of soil, Fv is the fractional vegetation cover derived from Eq. (3) (Sobrino et al., 2004), and $d\varepsilon$ is calculated using Eq. (8):

$$d\varepsilon = (1 - \varepsilon_s)(1 - \mathrm{Fv}) F \varepsilon_v \tag{8}$$

where F is the shape factor, which has a mean value of 0.55 for several different geometrical distributions (Sobrino et al., 2004).

As for HJ-1B IRS, the emissivities of soil and vegetation are 0.972 and 0.983, respectively (Zhou et al., 2011b). Taking into account Eqs. (7) and (8), ε can be expressed by Eq. (9):

$$\varepsilon = -0.004\mathrm{Fv} + 0.987 \tag{9}$$

The LST was calculated using the steps described above and is shown in Fig. 2(b).

Calculation of landscape metrics

In addition to NDVI and Fv, the effects of the spatial structure of land use on the UHI were quantitatively assessed using landscape metrics, which included four class-based metrics and three landscape-based metrics. The metrics for this study were chosen according to the following principles: (1) important in both theory and practice, (2) interpretable, (3) minimal redundancy, and (4) easily computed (Lee et al., 2009; Li and Wu, 2004; Riitters et al., 1995; Riva-Murray et al., 2010). The four class-based metrics were: (1) percentage of landscape (PLAND), (2) patch density (PD), (3) edge density (ED), and (4) landscape shape index (LSI). The three landscape-based metrics were: (1) contagion index (CONTAG), (2) Shannon's evenness index (SHEI) and (3) Shannon's diversity index (SHDI). All these landscape metrics, their definitions and their equations are listed in Table 2 (McGarigal et al., 2002).

The class level and landscape level metrics were derived from the professional FRAGSTATS software using the "8-cell rule" to define patch neighbors (McGarigal et al., 2002). To maintain a balance between the number of statistical samples and the computational burden, Wuhan was divided into 25 subplots that were

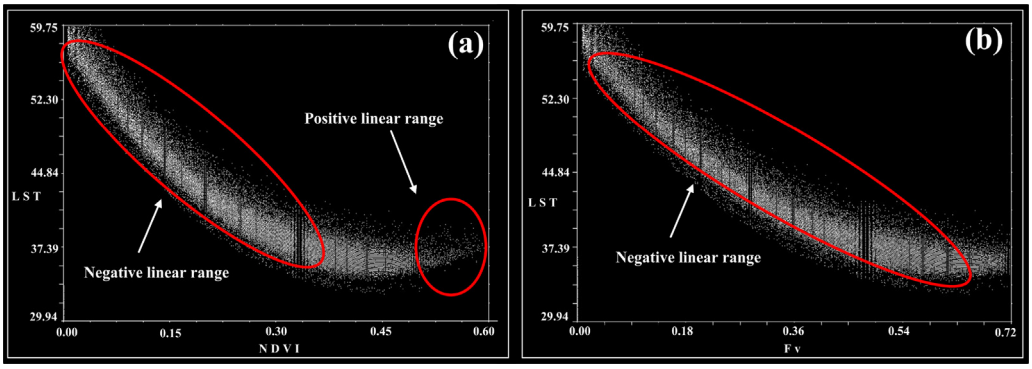

Fig. 4. Scatter grams of LST vs. NDVI and Fv for the study area: (a) LST vs. NDVI and (b) LST vs. Fv.

18.5 km × 18.5 km in size. The landscape metrics and the mean LST values of each land use type were calculated for each subplot. The Pearson's correlation coefficients between the landscape metrics and each of the mean LSTs were then computed and used to determine the impacts of the spatial structure of land use on the urban heat island. Because the values of the scaling terms in the test statistics were unknown and were replaced by estimates, their statistical significances ($p = 0.01$ and $p = 0.05$) were determined using a two-tailed Student's t-test. It is noted that the Pearson's correlation coefficients from a two-tailed Student's t-test are just calculated on two variables of the landscape metrics and each of the mean LSTs. This is an ordinary significance test between land use spatial structure and its temperature, not for the heat island center.

Fractal analysis

Previous studies of UHIs mainly used fractal analysis as an effective spatial measure to describe spatial features of the land surface temperature (Weng, 2003; Weng and Yang, 2004). However, we incorporated the radius fractal dimension into the analysis of the spatial variation of different land use types associated with the urban heat island to improve the understanding of the distinctive thermal features of different land use types.

Several effective methods have been developed to transcribe fractal theory into concrete algorithms, including the box counting method, the pixel dilation method, the caliper method, and the mass–radius method (Batty and Longley, 1987; Fernández and Jelinek, 2001; Frankhauser, 1997). We used the mass–radius method to determine the radius fractal dimension. This method consists of covering patches of land with circles of radius r and then counting the total area of the patches intercepted by the circle as its radius increases (Backes and Bruno, 2013; Wu et al., 2013). Using the correlation between the total patch area and the radius with respect to a certain land use type, the radius fractal dimension can be calculated to depict the density change from the urban center to the rural areas. Although the geometric center of the urban area is usually used as the center of the analysis, it is more reasonable for the center of the hot area to be regarded as the center of measurement when examining the effects of the spatial structure of land use on the urban heat island. We then used the neighborhood statistics to extract the hot centers and the buffer zone to obtain the areas of various land use types for every hot center with the ArcGIS software. Because only a limited range of each hot center is affected by the UHI, it was meaningless to consider the urban land patches that were located far from every hot center. At present, there are about 50 weather stations within its central district that covers 888 km^2 in Wuhan, which shows that there is a weather station per 17 km^2. It means that the interval for weather station is 4000 m that has the same distribution as Shanghai. In addition, the regression analysis related to fractal dimension is required to need enough sample size (not less than 30) to achieve a more accurate estimation. Therefore, we only analyzed the contributions of the land use types to the UHI at distances between 100 m and 4000 m. The buffer analysis was used to add the proportion of the five land use types in each 100 m increment of radius. A mean LST value was computed from all the corresponding pixels in each increment. The area $S(r)$ for a certain land use type within a buffer zone can be calculated as:

$$S(r) = \eta r^{D_r} \tag{10}$$

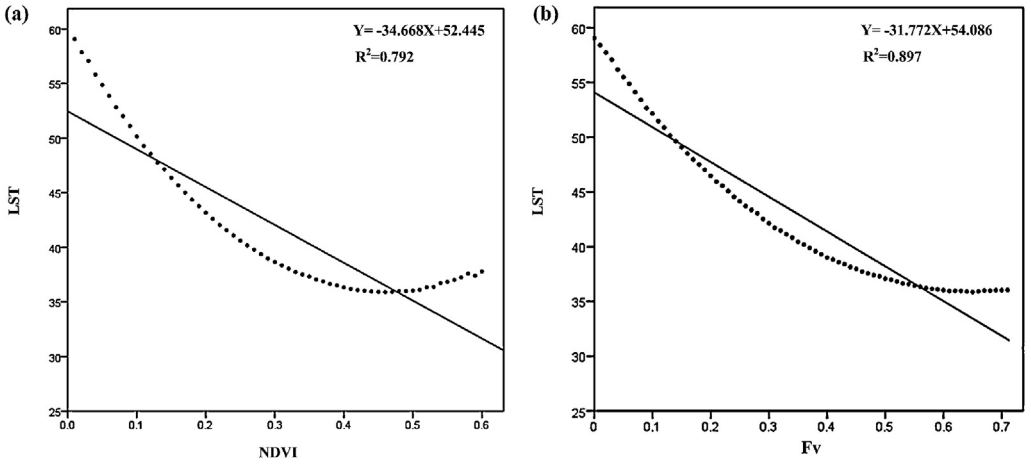

Fig. 5. Relationship of mean LST vs. NDVI and Fv for the study area: (a) regression analysis between LST and positive NDVI and (b) regression analysis between LST and Fv.

where η is a coefficient and D_r is the radius fractal dimension. The radius fractal dimension D_r of a certain land use type measures the change in density from the hot center to its edge. Eq. (10) was simplified by natural logarithms as follows:

$$\ln\ S(r) = \ln\ \eta + D_r\ \ln\ r \tag{11}$$

By using linear least square fitting, we can easily calculate the radius fractal dimensions from Eq. (11). When $D_r < 2$, the spatial density of the measured patches for a certain land use type decreases nonlinearly from the hot center to the edge. The decrease occurs more quickly with smaller values of D_r. However, when $D_r > 2$, the spatial density increases from the hot center to the edge. When $D_r = 2$, the spatial density remains unchanged from the hot center to the edge. A detailed computation of radius fractal dimensions was performed by (Wu et al., 2008, 2013).

Results and discussion

Relationship between the urban heat island and NDVI and Fv

Fig. 3(a) shows the distribution of NDVI for Wuhan. The values of NDVI range from −0.429 to 0.600 and have a mean value of 0.078 and a standard deviation of 0.158. The distribution shows that the orange areas correlate with the high LST values in Fig. 2(b). NDVI has been regarded as the key biophysical factor in the formation of UHIs in previous studies (Yang et al., 2010; Zhang et al., 2009). Although NDVI has been demonstrated to have a nonlinear

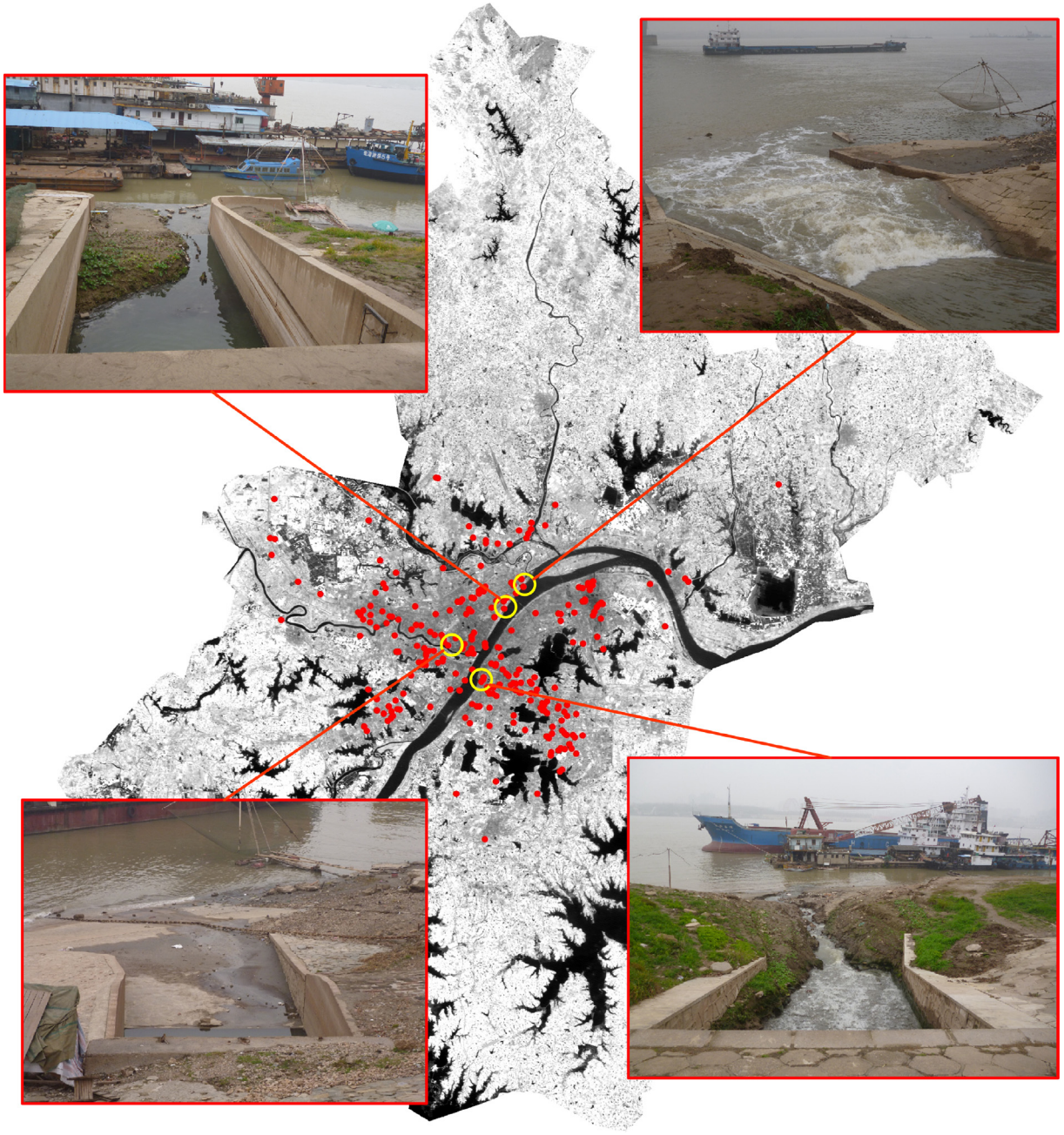

Fig. 6. Distribution map of 251 hot spots for the study area. Note four typical central district scenes about direct heat releases from industrial effluent or sanitary sewage are particularly shown.

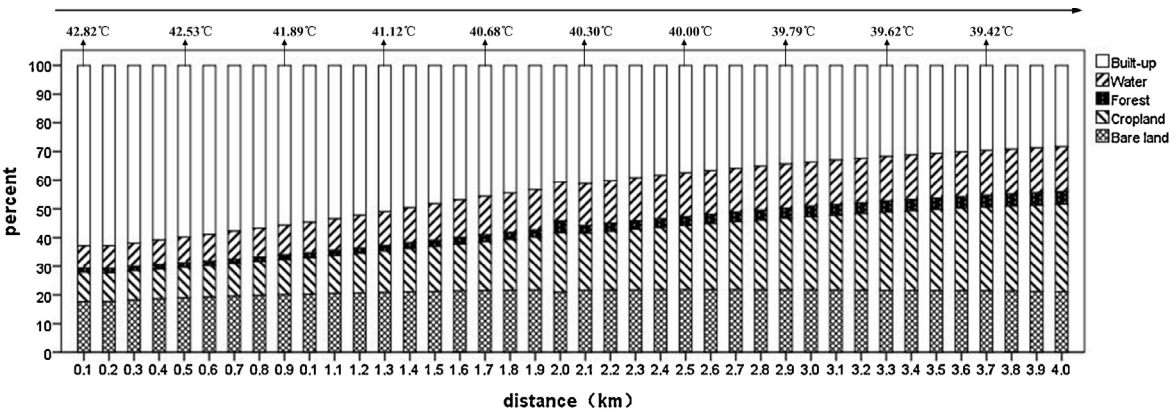

Fig. 7. Area percentage of each land use category and mean LST variation around all hot spots within an extension of 4000 m.

correlation with mean LST across the entire range of NDVI values, there is a significant negative linear correlation between mean LST and positive NDVI, which is caused by the presence of vegetation (Fig. 4(a)). Negative NDVI values have no physical meaning because the pixel is usually a mixture of non-vegetation components, such as clouds, water, or snow. Consequently, we limit our study of the relationship between NDVI and LST to positive NDVI values. The regression lines with negative correlations between NDVI and mean LST in Fig. 5(a) are only based on positive NDVI values. However, it is interesting to note that there is a positive linear correlation between NDVI and LST when NDVI is greater than 0.5 (Fig. 4(a)) in locations of 100% vegetation cover. This observation has been documented extensively in the remote sensing literature (Chen et al., 2006; Li et al., 2011).

Fv, which is another biophysical land surface parameter, varies from 0 to 1 and is also often used to represent vegetation abundance. Previous studies have indicated that Fv is strongly related to LST values that are retrieved from remote sensing images (Li et al., 2011). To further validate the performance of the HJ-1B satellite for monitoring UHIs, we used scatter plots to estimate the relationships between LST and Fv; these plots are shown in Figs. 4(b) and 5(b). Fig. 4(b) shows that Fv is negatively correlated across the entire range of values, while the negative relationship between NDVI and LST shown in Fig. 4(a) only exists for NDVI values less than 0.5. When NDVI is greater than 0.5, there is a positive correlation, which is an obstacle to exploring the relationship between LST and vegetation abundance. Fig. 5(b) shows a strong and clear regression relationship ($R^2 = 0.897$) between Fv and LST, while a weak relationship ($R^2 = 0.792$) with NDVI is shown in Fig. 5(a). This supports the general assessment that Fv is a better predictor of land surface temperature than NDVI for forested land covers. The same relationships between LST and NDVI as well as Fv have been identified by several studies (Carlson and Ripley, 1997; Song, 2005). Similar to remote sensor satellites such as Landsat, NOAA and MODIS, it can be demonstrated that HJ-1B data can be used to accurately assess the correlation between LST and vegetation abundance. However, the HJ-1B satellite passes over China once every four days, which is more frequent than other remote sensing satellites. Hence, the HJ-1B satellite is more suitable for monitoring UHIs in the major metropolises in China.

Table 3
Pearson's correlation coefficients between land surface temperature and class-level pattern metrics.

	PLAND	PD	ED	LSI
Built-up	.813**	.791*	.806*	.124
Water	−.630**	−.388	−.399*	−.109
Forest	−.593**	−.632**	.204	−.490*
Cropland	−.676*	−.619*	−.271	.232

* Correlation is significant at the 0.05 level (2-tailed).
** Correlation is significant at the 0.01 level (2-tailed).

Relationship between the urban heat island and landscape metrics

The correlation coefficients between the land surface temperature and the landscape metrics at the class and landscape levels are shown in Tables 3 and 4. Although previous studies have shown that bare land can comprise a major component of the urban surface and the UHI (Li et al., 2012b), bare land has a weak effect on the UHI in Wuhan because of its scattered distribution and small patch size and can be ignored in the statistical analysis. In this study, the other four dominant land use types, including built-up areas, cropland, forest and water, were taken into account in the correlation analysis of the class-level metric analysis.

In Wuhan, LST is highly related to the landscape metrics of built-up areas, cropland, forest, and water. The mean LST of forest is negatively correlated to PLAND, PD and LSI, indicating the cooling effect of vegetation on the UHI. However, the mean LST is positively correlated to PLAND, PD and ED for built-up areas because of the high heat capacity and thermal conductivity of the surface materials. An interesting and important finding is the negative relationships between mean LST and PLAND as well as ED for water. These relationships suggest that water has a significant effect on mitigating the UHI in Wuhan, which is different from many other metropolises in China such as Beijing, Shanghai, Chongqing and Changsha (Li et al., 2011; Liu and Deng, 2011; Li and Yu, 2014; Chen et al., 2008). Water has the largest specific heat among all the land use classes and is thus the most effective material for cooling the land. However, no correlations exist between mean LST and the landscape metrics, such as PLAND (0.104) and ED (0.147), in water areas in Shanghai (Li et al., 2011), while the mean LST is significantly correlated with PLAND (−0.630**) and ED (−0.399*) in Wuhan. Two geographical factors may cause this difference. First, water accounts for more than 25% of the area of the central district in Wuhan. In particular, East Lake, which is located in northeastern Wuhan, is the largest urban lake in the central districts of China. Second, dozens of other large lakes, such as South Lake, Sha Lake

Table 4
Pearson's correlation coefficients between land surface temperature and landscape-level pattern metrics.

CONTAG	SHDI	SHEI
.630**	−.613**	−.567**

** Correlation is significant at the 0.01 level (2-tailed).

and Hou Lake, are located in different parts of Wuhan. The Yangtze River and Han River also flow through the city center and divide the central districts into three regions. These water bodies, together with wetlands, fish ponds, and other rivers and lakes, are homogeneously distributed across the study area, which implies that the spatial distribution of water has a significant effect on the UHI. These results show that both the area and distribution of water are major causes for the differences between the UHIs in Wuhan and other large cities in China.

This study also demonstrates that LST is correlated to not only the landscape composition but also the spatial configuration. The mean LST is negatively correlated to SHDI and SHEI (Table 4). This indicates that the greater the number of land use types there are, and the more equal their abundances are, the more beneficial they are for relieving the urban heat island effect. In contrast, the mean LST shown in Table 4 is positively related to the contagion index, which measures both patch type interspersion as well as patch dispersion at the landscape level. This means that landscapes with a few large and contiguous patches will result in high values of contagion, which leads to a significant urban heat island effect and vice versa. Both of these results agree with the fact that a mixture of land use types and spatial patterns (e.g., the impervious surface areas and other land use types) will reduce the UHI effect. This result can also be derived from Landsat ETM+ (Li et al., 2011) and reveals that HJ-1B data have comparable performance to Landsat data in examining UHIs.

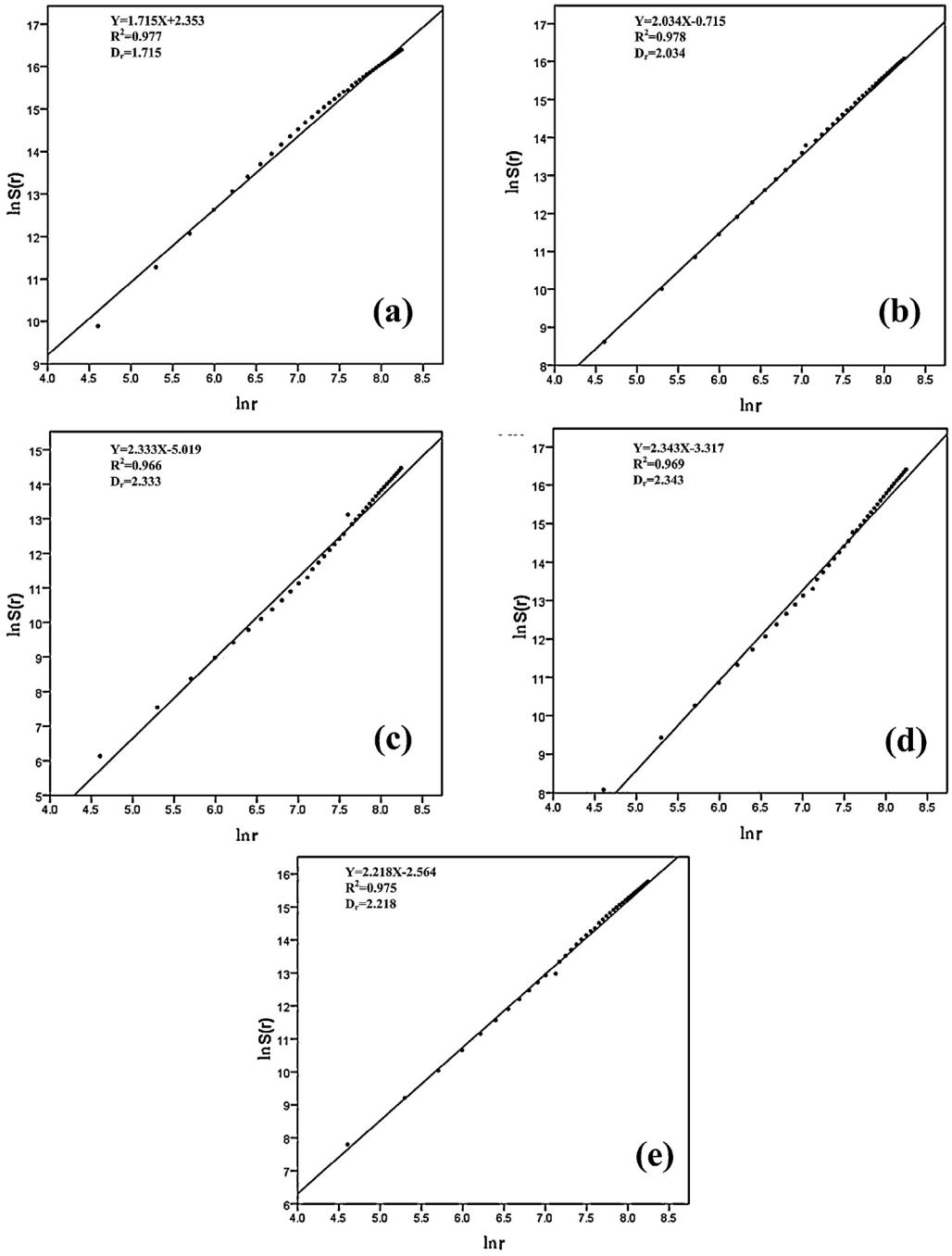

Fig. 8. The log-log plots used to extract fractal dimensions of five different land use types scattering from hot centers in Wuhan: (a) built-up; (b) bare land; (c) forest; (d) cropland and (e) water.

Contributions of different land use types to the urban heat island effect

Given that LST varies with land use type as demonstrated above, we extracted the hot centers of the urban heat island. As shown in Fig. 6, 87.6% of the hot centers are located in built-up areas, which is similar to other large cities (e.g., Shanghai and Beijing). However, 6% of the hot centers are near areas of water. Field investigations show that these hot centers are not natural water areas but are areas of industrial effluent or sanitary sewage, which suggests that the direct releases of heat from industry and urban society play important roles in localized temperature increases but are often ignored.

From the statistical point of view, Fig. 7 shows that the temperatures tend to decrease from the hot centers to the edges of the region. The temperature difference between the buffer zones that are 0.1 km and 4 km from the hot centers is almost 4 °C. Around the hot centers (0–500 m), the proportion of built-up areas is more than 60%, while the total proportion of forest, cropland and water areas is less than 20%. In contrast, far from the hot centers (3000–4000 m), the proportion of built-up areas is less than 30%, and the total proportion of forest, cropland and water areas is more than 50%. These results indicate that the areas with high concentrations of buildings often lead to the formation of heat island centers, while forest, cropland and water are beneficial to mitigating UHI.

To quantitatively analyze the effects of the spatial structure of land use on the UHI, we integrated the buffer analysis with the radius fractal dimension. Statistically significant ($p < 0.001$) correlations between the percentage of land use types and the radius were then established with conventional regression analyses. Fig. 8 shows that there is a high correlation between the radius and area for all five land use types. The slope of a fitted line shown in Fig. 8 is the radius fractal dimension (D_r) for a given land use type. From this figure, we can find that the radius fractal dimensions of the urban land use types are ranked as cropland, forest, water, bare land and built-up areas in descending order. Among the five land use types, only the radius fractal dimension of the built-up area is less than 2 (1.715). This further suggests that the density of built-up areas sharply decreases away from the hot centers, which implies that built-up areas are the main contributors to the temperature increase. The radius fractal dimension of bare land is closer to 2 (2.034) than the other four land use types, which implies that the bare land is evenly distributed around the hot centers and that its distribution has little effect on the change in UHI intensity. Conversely, the radius fractal dimensions of water, forest and cropland are 2.218, 2.333 and 2.343, respectively. All of these are greater than 2, which indicate that the densities of water, forest, and cropland increase with increasing distance from the hot centers. This reveals that the water and forest, and especially water, have significant effects on cooling the land in the study site.

Conclusions

This study demonstrated that the newly launched HJ-1B satellite, which has a high spectral resolution, medium-high spatial resolution and stable radiation properties, is comparable to other remote sensing satellites such as Landsat and MODIS in terms of monitoring the UHI. Most important for government officials and researchers, the HJ-1B satellite has a 4-day revisiting frequency and a 300-m spatial resolution, so it is more suitable to examine the spatial characteristics of UHIs in near real time than Landsat as well as in assessment accuracy than MODIS. Although HJ-1B data have been used to examine the effects of the spatial structure of land use on urban heat islands, the ways to utilize various biophysical indices, such as NDVI, Fv and landscape metrics, to test the performance of the HJ-1B thermal infrared band for monitoring UHIs have not been addressed. Our study of HJ-1B remote sensing imagery in Wuhan sheds some light on this issue.

The mean LST derived from the HJ-1B data can help us understand the variations in thermal response to different surface materials. The results suggest that the distribution of the UHI is related to the built-up areas. Built-up areas are usually located in the urban center and occur in zones of high LST values. Previous studies have reported that Wuhan has experienced an ongoing and accelerated urbanization; the built-up area has increased by 303.14% over the last two decades (Xie et al., 2012). This has caused the increased density and expansion of the urban built-up area, which resulted in the UHI. The results reveal that urbanization plays a major role in the regional UHI. In contrast, the forest areas, which are mostly located in the suburbs of Wuhan, have the lowest temperatures and are more effective in mitigating the UHI effect. This should encourage designers and government officials to devote more efforts in protecting forests. The comparisons between Wuhan and other large cities in China show that the significant differences in the effect of the spatial structure of land use on the urban heat island are due to the area and spatial distribution of water bodies. Hence, the protection of water bodies is also important to mitigating the UHI in those cities that, like Wuhan, contain many water bodies. However, water relieves the UHI only under certain conditions. Wuhan has abundant surface water resources (over one quarter of the central district) and a homogeneous spatial distribution. It should be noted that both of these are major factors for water to mitigate the UHI. This limitation deserves further examination in future analyses because some large cities in northern China do not contain as many bodies of water as Wuhan.

The utility of the radius fractal dimension to analyze the spatial patterns of urban land use around the hot centers in Wuhan proved to be more comprehensive than other biophysical indices. Although our analysis also found a strong linear relationship between LST and the vegetation indices (NDVI and Fv), the variation of the UHI was confined to forest and cropland rather than other land use types. Furthermore, the vegetation indices are significantly affected by the image resolution because they require a pixel-by-pixel examination. In comparison, landscape pattern metrics are more comprehensive than vegetation indices because they can adapt to all land use types and perform preliminary spatial correlations by patches instead of pixels. This has significantly facilitated the study of landscape metrics in response to the spatial distribution of the UHI. However, assessing the effects of the spatial structure of land use on the urban heat island using landscape metrics can only confirm the relevance between them but cannot quantify the corresponding spatial strength. The generation of the UHI is attributed to significant spatial differences of thermal energy accumulation in the urban area, which leads to higher temperatures in the central urban districts than rural areas. Therefore, to further advance our understanding of the variation of UHI response to different spatial structures of land use, it is critically important to use the radius fractal dimension to characterize the spatial pattern of the thermal environment across a range of urban areas.

As has been noted by Weng (2003), the spatial arrangement and area of different land use types are fundamental factors in the modification of the spatial structures of UHIs. Different spatial structures of land use have different effects on UHIs, which has important implications for urban land use planning and design to mitigate UHIs. However, we concur with other researchers that multiple methods should be used wherever possible to allow for a thorough exploration. In the future, additional spatial analysis methods should be developed to examine the spatial patterns of land use from other perspectives and to downscale HJ-1B TIR data for UHI evaluations. This will assist governments and researchers

in gaining deeper insight into the complex thermal heterogeneity of urban land use.

Acknowledgments

This work is supported by the National Natural Science Foundation of China (40901214), the China Postdoctoral Science Foundation (2013M531749 and 2012T50691), the Hong Kong Scholars Program (XJ2012036), the Hong Kong Polytechnic University under Projects(G-YZ26), the Wuhan Youth Chenguang Program of Science and Technology (201150431093), the Fundamental Research Funds for the Central Universities (2013-IV-040), the Independent Innovation Research Fund of Wuhan University of Technology (126608001) and the self-determined and innovative research funds of WUT (136608001, 136808004 and 20131049708001). We would like to thank CRESDA for providing us with the HJ-1B image. Also, we thank Xiaojun Zhao, Yanghui Gao, Nanshan You, Qiang Wang, Xiuqing Tian and Yan Li for their assistance during the field investigations. We are grateful to American Journal Experts for English editing of the manuscript.

References

Aguiar, R., Oliveira, M., Gonccedilalves, H., 2002. Climate change impacts on the thermal performance of Portuguese buildings. Results of the SIAM study. Build. Serv. Eng. Res. Technol. 23 (4), 223–231.

Arnfield, A.J., 2003. Two decades of urban climate research: a review of turbulence, exchanges of energy and water, and the urban heat island. Int. J. Climatol. 23 (1), 1–26.

Backes, A.R., Bruno, O.M., 2013. Texture analysis using volume–radius fractal dimension. Appl. Math. Comput. 219 (11), 5870–5875.

Batty, M., Longley, P.A., 1987. Fractal-based description of urban form. Environ. Plan. B: Plan. Des. 14 (2), 123–134.

Carlson, T.N., Ripley, D.A., 1997. On the relation between NDVI, fractional vegetation cover, and leaf area index. Remote Sens. Environ. 62 (3), 241–252.

Chen, F., He, B.Y., Long, Z.Y., Yang, X.Q., 2008. A Spatial analysis of urban heat island and unerlying surface using Landsat ETM+. Remote Sens. Land Resour. 20 (2), 56–61.

Chen, X.L., Zhao, H.M., Li, P.X., Yin, Z.Y., 2006. Remote sensing image-based analysis of the relationship between urban heat island and land use/cover changes. Remote Sens. Environ. 104 (2), 133–146.

Chen, Y., Sui, D.Z., Fung, T., Dou, W., 2007. Fractal analysis of the structure and dynamics of a satellite-detected urban heat island. Int. J. Remote Sens. 28 (10), 2359–2366.

Cui, Y.Y., De Foy, B., 2012. Seasonal variations of the urban heat island at the surface and the near-surface and reductions due to urban vegetation in Mexico City. J. Appl. Meteorol. Climatol. 51 (5), 855–868.

Dousset, B., Gourmelon, F., 2003. Satellite multi-sensor data analysis of urban surface temperatures and landcover. ISPRS – J. Photogramm. Remote Sens. 58 (1–2), 43–54.

Fernández, E., Jelinek, H.F., 2001. Use of fractal theory in neuroscience: methods advantages, and potential problems. Methods 24 (4), 309–321.

Frankhauser, P., 1997. The fractal approach: a new tool for the spatial analysis of urban agglomerations. Population 52 (4), 1005–1040.

Friedl, M.A., McIver, D.K., Hodges, J.C.F., Zhang, X.Y., Muchoney, D., Strahler, A.H., Woodcock, C.E., Gopal, S., Schneider, A., Cooper, A., Baccini, A., Gao, F., Schaaf, C., 2002. Global land cover mapping from MODIS: algorithms and early results. Remote Sens. Environ. 83 (1–2), 287–302.

Gallo, K.P., Owen, T.W., 1998. Assessment of urban heat Islands: a multi-sensor perspective for the Dallas-Ft. worth USA region. Geocarto Int. 13 (4), 35–41.

Gao, Z.Q., Gao, W., Chang, N.B., 2011. Integrating temperature vegetation dryness index (TVDI) and regional water stress index (RWSI) for drought assessment with the aid of Landsat TM/ETM plus images. Int. J. Appl. Earth Obs. Geoinf. 13 (3), 495–503.

Hage, K., 2003. On destructive Canadian prairie windstorms and severe winters – a climatological assessment in the context of global warming. Nat. Hazards 29 (2), 207–228.

Herzog, F., Lausch, A., 2001. Supplementing land-use statistics with landscape metrics: some methodological considerations. Environ. Monit. Assess. 72 (1), 37–50.

House-Peters, L.A., Chang, H., 2011. Modeling the impact of land use and climate change on neighborhood-scale evaporation and nighttime cooling: a surface energy balance approach. Landsc. Urban Plan. 103 (2), 139–155.

Jimenez-Munoz, J.C., Sobrino, J.A., 2003. A generalized single-channel method for retrieving land surface temperature from remote sensing data. J. Geophys. Res. 108, D22.

Kardinal Jusuf, S., Wong, N.H., Hagen, E., Anggoro, R., Hong, Y., 2007. The influence of land use on the urban heat island in Singapore. Habitat Int. 31 (2), 232–242.

Lee, S.W., Hwang, S.J., Lee, S.B., Hwang, H.S., Sung, H.C., 2009. Landscape ecological approach to the relationships of land use patterns in watersheds to water quality characteristics. Landsc. Urban Plan. 92 (2), 80–89.

Li, C., Yu, C.W., 2014. Mitigation of urban heat development by cool island effect of green space and water body. In: Li, A., Zhu, Y.X., Li, Y.G. (Eds.), Proceedings of the 8th International Symposium on Heating, Ventilation and Air Conditioning. Springer, Berlin, Heidelberg, pp. 551–561.

Li, H.B., Wu, J.G., 2004. Use and misuse of landscape indices. Landsc. Ecol. 19 (4), 389–399.

Li, J.J., Wang, X.R., Wang, X.J., Ma, W.C., Zhang, H., 2009. Remote sensing evaluation of urban heat island and its spatial pattern of the Shanghai metropolitan area China. Ecol. Complex. 6 (4), 413–420.

Li, J.X., Song, C.H., Cao, L., Zhu, F.G., Meng, X.L., Wu, J.G., 2011. Impacts of landscape structure on surface urban heat islands: a case study of Shanghai China. Remote Sens. Environ. 115 (12), 3249–3263.

Li, K., Yu, Z., 2008. Comparative and combinative study of urban heat island in wuhan city with remote sensing and CFD. Simul. Sensors. 8 (10), 6692–6703.

Li, X.M., Zhou, W.Q., Ouyang, Z.Y., Xu, W.H., Zheng, H., 2012a. Spatial pattern of greenspace affects land surface temperature: evidence from the heavily urbanized Beijing metropolitan area, China. Landsc. Ecol. 27 (6), 887–898.

Li, Y.Y., Zhang, H., Kainz, W., 2012b. Monitoring patterns of urban heat islands of the fast-growing Shanghai metropolis, China: using time-series of Landsat TM/ETM+ data. Int. J. Appl. Earth Obs. Geoinf. 19, 127–138.

Liang, B.Q., Weng, Q.H., 2011. Assessing urban environmental quality change of Indianapolis (1998) United States, by the remote sensing and GIS integration. IEEE J. Sel. Top. Appl. Earth Observ. Remote Sens. 4 (1), 43–55.

Liu, J.M., Deng, X.Z., 2011. Influence of different land use on urban microenvironment in Beijing City China. J. Food Agric. Environ. 9 (3&4), 1005–1011.

Lo, C.P., Quattrochi, D.A., 2003. Land-use and land-cover change, urban heat island phenomenon, and health implications: a remote sensing approach. Photogramm. Eng. Remote Sens. 69 (9), 1053–1063.

Ma, Y., Kuang, Y., Huang, N., 2010. Coupling urbanization analyses for studying urban thermal environment and its interplay with biophysical parameters based on TM/ETM+ imagery. Int. J. Appl. Earth Obs. Geoinf. 12 (2), 110–118.

Mallick, J., Singh, C.K., Shashtri, S., Rahman, A., Mukherjee, S., 2012. Land surface emissivity retrieval based on moisture index from Landsat TM satellite data over heterogeneous surfaces of Delhi city. Int. J. Appl. Earth Obs. Geoinf. 19, 348–358.

McGarigal, K., Cushman, S., Neel, M., Ene, E., 2002. FRAGSTATS: spatial pattern analysis program for categorical maps. Computer software program produced by the authors at the University of Massachusetts, Amherst., Available at the following web site. www.umass.edu/landeco/research/fragstats/fragstats.html

Oke, T.R., 1973. City size and the urban heat island. Atmos. Environ. (1967) 7 (8), 769–779.

Riitters, K.H., O'Neill, R.V., Hunsaker, C.T., Wickham, J.D., Yankee, D.H., Timmins, S.P., Jones, K.B., Jackson, B.L., 1995. A factor analysis of landscape pattern and structure metrics. Landsc. Ecol. 10 (1), 23–39.

Riva-Murray, K., Riemann, R., Murdoch, P., Fischer, J.M., Brightbill, R., 2010. Landscape characteristics affecting streams in urbanizing regions of the Delaware River Basin (New Jersey, New York, and Pennsylvania, U.S.). Landsc. Ecol. 25 (10), 1489–1503.

Roy, P.S., Padalia, H., Chauhan, N., Porwal, M.C., Gupta, S., Biswas, S., Jagdale, R., 2005. Validation of geospatial model for biodiversity characterization at landscape level – a study in Andaman & Nicobar Islands India. Ecol. Model. 185 (2–4), 349–369.

Saaroni, H., Ben-Dor, E., Bitan, A., Potchter, O., 2000. Spatial distribution and microscale characteristics of the urban heat island in Tel-Aviv, Israel. Landsc. Urban Plan. 48 (1–2), 1–18.

Salisbury, J.W., D'Aria, D.M., 1992. Emissivity of terrestrial materials in the 8–14 μm atmospheric window. Remote Sens. Environ. 42, 83–106.

Sobrino, J.A., Jimenez-Munoz, J.C., Paolini, L., 2004. Land surface temperature retrieval from Landsat TM 5. Remote Sens. Environ. 90 (4), 434–440.

Sobrino, J.A., Oltra-Carrio, R., Jimenez-Munoz, J.C., Julien, Y., Soria, G., Franch, B., Mattar, C., 2012. Emissivity mapping over urban areas using a classification-based approach: application to the Dual-use European Security IR Experiment (DESIREX). Int. J. Appl. Earth Obs. Geoinf. 18, 141–147.

Sobrino, J.A., Raissouni, N., Li, Z.L., 2001. A comparative study of land surface emissivity retrieval from NOAA data. Remote Sens. Environ. 75 (2), 256–266.

Song, C.H., 2005. Spectral mixture analysis for subpixel vegetation fractions in the urban environment: how to incorporate endmember variability? Remote Sens. Environ. 95 (2), 248–263.

Streutker, D.R., 2002. A remote sensing study of the urban heat island of Houston, Texas. Int. J. Remote Sens. 23 (13), 2595–2608.

Streutker, D.R., 2003. Satellite-measured growth of the urban heat island of Houston, Texas. Remote Sens. Environ. 85 (3), 282–289.

Taha, H., 1997. Urban climates and heat islands: albedo, evapotranspiration, and anthropogenic heat. Energy Build. 25 (2), 99–103.

Tan, K.C., Lim, H.S., MatJafri, M.Z., Abdullah, K., 2012. A comparison of radiometric correction techniques in the evaluation of the relationship between LST and NDVI in Landsat imagery. Environ. Monit. Assess. 184 (6), 3813–3829.

Tran, H., Uchihama, D., Ochi, S., Yasuoka, Y., 2006. Assessment with satellite data of the urban heat island effects in Asian mega cities. Int. J. Appl. Earth Obs. Geoinf. 8 (1), 34–48.

Turkoglu, N., 2010. Analysis of urban effects on soil temperature in Ankara. Environ. Monit. Assess. 169 (1–4), 439–450.

Van De Kerchove, R., Lhermitte, S., Veraverbeke, S., Goossens, R., 2013. Spatio-temporal variability in remotely sensed land surface temperature, and its

relationship with physiographic variables in the Russian Altay Mountains. Int. J. Appl. Earth Obs. Geoinf. 20, 4–19.
Voogt, J.A., Oke, T.R., 2003. Thermal remote sensing of urban climates. Remote Sens. Environ. 86 (3), 370–384.
Wang, Q., Zhao, S.H., Zhang, F., Yang, H.J., Nie, Y.H., Liu, S.H., Li, Y. CN 102103203 A (2011) (in Chinese).
Wang, Q.A., Wu, C.Q., Li, Q., Li, J.S., 2010. Chinese HJ-1A/B satellites and data characteristics. Sci. China-Earth Sci. 53, 51–57.
Weng, Q., 2001. A remote sensing-GIS evaluation of urban expansion and its impact on surface temperature in the Zhujiang Delta China. Int. J. Remote Sens. 22 (10), 1999–2014.
Weng, Q., 2003. Fractal analysis of satellite-detected urban heat island effect. Photogramm. Eng. Remote Sens. 69 (5), 555–566.
Weng, Q., Lu, D.S., Schubring, J., 2004. Estimation of land surface temperature-vegetation abundance relationship for urban heat island studies. Remote Sens. Environ. 89 (4), 467–483.
Weng, Q., Yang, S.H., 2004. Managing the adverse thermal effects of urban development in a densely populated Chinese city. J. Environ. Manage. 70 (2), 145–156.
Weng, Q.H., Liu, H., Liang, B.Q., Lu, D.S., 2008. The spatial variations of urban land surface temperatures: pertinent factors zoning effect, and seasonal variability. IEEE J. Sel. Top. Appl. Earth Observ. Remote Sens. 1 (2), 154–166.
Weng, Q.H., Lu, D.S., 2008. A sub-pixel analysis of urbanization effect on land surface temperature and its interplay with impervious surface and vegetation coverage in Indianapolis United States. Int. J. Appl. Earth Obs. Geoinf. 10 (1), 68–83.
Weng, Y.C., 2007. Spatiotemporal changes of landscape pattern in response to urbanization. Landsc. Urban Plan. 81 (4), 341–353.
Wilson, J.S., Clay, M., Martin, E., Stuckey, D., Vedder-Risch, K., 2003. Evaluating environmental influences of zoning in urban ecosystems with remote sensing. Remote Sens. Environ. 86 (3), 303–321.
Wu, H., Chen, X.L., Cai, X.B., Dai, J.Z., Li, Q.Q., 2008. Research on spatio-temporal evolution of land use based on compositive fractal model. J. Wuhan Univ. Technol. 30 (1), 154–157.
Wu, H., Cheng, Z.P., Shi, W.Z., Miao, Z.L., Xu, C.C., 2014. An object-based image analysis for building seismic vulnerability assessment using high-resolution remote sensing imagery. Nat. Hazards 71 (1), 151–174.
Wu, H., Sun, Y.R., Shi, W.Z., Chen, X.L., Fu, D.J., 2013. Examining the satellite-detected urban land use spatial patterns using multidimensional fractal dimension indices. Remote Sens. 5 (10), 5152–5172.
Wu, H., Zhou, L., Chi, X., Li, Y., Sun, Y.R., 2012. Quantifying and analyzing neighborhood configuration characteristics to cellular automata for land use simulation considering data source error. Earth Sci. Inform. 5 (2), 77–86.
Xian, G., Crane, M., 2006. An analysis of urban thermal characteristics and associated land cover in Tampa Bay and Las Vegas using Landsat satellite data. Remote Sens. Environ. 104 (2), 147–156.
Xie, Q.J., Zhou, Z.X., Teng, M.J., Wang, P.C., 2012. A multi-temporal Landsat TM data analysis of the impact of land use and land cover changes on the urban heat island effect. J. Food Agric. Environ. 10 (2), 803–809.
Xu, H.Q., Ding, F., Wen, X.L., 2009. Urban expansion and heat island dynamics in the Quanzhou Region, China. IEEE J. Sel. Top. Appl. Earth Observ. Remote Sens. 2 (2), 74–79.
Yang, J., Gong, P., Zhou, J.X., Huang, H.B., Wang, L., 2010. Detection of the urban heat island in Beijing using HJ-1B satellite imagery. Sci. China-Earth Sci. 53 (Suppl. I), 67–73.
Ye, L.P., Wu, H., Li, Y., Zhao, X.J., Zhang, J.W., You, N.S., Cui, W., Huang, J.J., 2013. A study on the thermal environmental effect of urban land use based on fractal theory – a case of Wuhan City. J. Central China Normal Univ. Nat. Sci. 47 (4), 578–582.
Yu, Z.F., Chen, X.L., Zhou, B., Tian, L., Yuan, X.H., Feng, L., 2012. Assessment of total suspended sediment concentrations in Poyang Lake using HJ-1A/1B CCD imagery. Chin. J. Oceanol. Limnol. 30 (2), 295–304.
Zhang, Y.S., Odeh, I.O.A., Han, C.F., 2009. Bi-temporal characterization of land surface temperature in relation to impervious surface area NDVI and NDBI, using a sub-pixel image analysis. Int. J. Appl. Earth Obs. Geoinf. 11 (4), 256–264.
Zhao, H., Chen, X., Zhang, J., Yin, Z., 2012. Land-use/-cover change spatial patterns and their impacts on sediment charge in the Longchuan River catchment, southwestern China. Int. J. Remote Sens. 33 (14), 4527–4552.
Zhao, S.H., Qin, Q.M., Zhang, F., Wang, Q., Yao, Y.J., You, L., Jiang, H.B., Cui, R.B., Yao, Y.J., 2011. Research on using a mono-window algorithm for land surface temperature retrieval from Chinese satellite for environment and natural disaster monitoring (HJ-1B) data. Spectrosc. Spectr. Anal. 31 (6), 1552–1556.
Zhou, J., Chen, Y.H., Wang, J.F., Zhan, W.F., 2011a. Maximum Nighttime Urban Heat Island (UHI) intensity simulation by integrating remotely sensed data and meteorological observations. IEEE J. Sel. Top. Appl. Earth Observ. Remote Sens. 4 (1), 138–146.
Zhou, J., Li, J., Zhao, X.A., Zhan, W.F., Guo, J.X., 2011b. A modified single-channel algorithm for land surface temperature retrieval from HJ-1B satellite data. J. Infrared Millim. Waves 30 (1), 61–67.